Turbulent Buoyant Flow and Pressure Variations around an Aircraft Fuselage in a Cross Wind near the Ground

H. S. KOU and K. T. YANG
Department of Aerospace and Mechanical Engineering
University of Notre Dame
Notre Dame, Indiana 46556, USA

J. R. LLOYD
Department of Mechanical Engineering
Michigan State University
East Lansing, Michigan 48824, USA

ABSTRACT

Two-dimensional numerical finite-difference calculations have been carried out to study the effects of cross wind speeds and the elevation of the fuselage on turbulent buoyant flow and pressure variations around an aircraft fuselage engulfed in a simulated fire in a uniform cross wind near the ground. Detailed velocity, temperature, smoke concentration, and pressure fields have been obtained and it is found that a major influence on the physical phenomena is the relative strength of the cross flow and the buoyant flow.

INTRODUCTION

In survivable aircraft accidents involving fires, there is a critical need to understand and predict flow of hot toxic gases inside the aircraft cabins. While the fire may be initiated inside the cabin, there is an equally important accident scenario in which a fire is initiated outside the fuselage due to fuel spill and spreads into the cabin through an opening (Emmons, 1982). In the latter scenario, the fire spread into the cabin is dictated by the flow and pressure fields surrounding the fuselage, which in turn depend on the location and strength of the fire source, the elevation of the fuselage, and the speed of the prevailing wind. The development of appropriate predictive schemes for such a scenario can ultimately provide needed inputs to the eventual development of fire-safety countermeasures. The purpose of this paper is to present some results of a recent numerical study addressing this very scenario to determine the physical effects of the various parameters on the flow and pressure fields surrounding the fuselage (Kou, 1984).

Similar to an earlier companion study dealing with fire and smoke spread inside aircraft cabins (Yang et al, 1984), the numerical computations are based on a two-dimensional, primitive-variable, differential field model which includes the effects of strong buoyancy, turbulence and compressibility. Flow, temperature, and smoke concentration fields are all calculated. An algebraic turbulence model which accommodates both local and stratification effects has been utilized. The fire located outside the fuselage, which is approximated by a circular cylinder, is simulated by a volumetric heat and smoke source with arbitrarily prescribed flame envelope and rates of local heat and smoke

---

H. S. Kou is currently at the Tatung Institute of Technology, Taipei, Taiwan, Republic of China.

generation. Calculations have been carried out for a fixed fire and smoke source which simulates the full-scale fire tests conducted at the Technical Center of the U. S. Federal Aviation Administration, but varying fuselage elevations and prevailing wind speeds.

MATHEMATICAL FORMULATION AND NUMERICAL ANALYSIS

Figure 1 depicts the configuration for the solution field where a cylindrical coordinate system is employed in the vicinity of the simulated fuselage, and the far region away from the fuselage is represented by a Cartesian coordinate system. The prevailing wind is at a uniform speed U_0. For the speeds considered in this study, the turbulent wall layer next to the ground is very thin, and therefore is neglected. The flame envelope on the ground, which represents the fire and smoke source, is taken to simulate a real fire, and its dimension and strengths will be described later. The Cartesian coordinate system has its origin located at the left lower corner of the solution field. The origin of the cylindrical coordinate system is located at the center of the circular cylinder (simulated fuselage).

The conservation field equations for mass, momentum, energy and smoke concentration in terms of flux quantities are well known in both coordinate systems. For illustrative purposes, these equations in Cartesian coordinates can be non-dimensionalized by introducing the following definitions:

$$X = \frac{\bar{X}}{D}, \quad Y = \frac{\bar{Y}}{D}, \quad t = \frac{U_0 \bar{t}}{D}, \quad U = \frac{\bar{U}}{U_0}, \quad V = \frac{\bar{V}}{U_0}, \quad T = \frac{\bar{T}}{T_0}$$

$$\rho = \frac{\bar{\rho}}{\rho_0}, \quad \rho_\epsilon = \frac{\bar{\rho}_\epsilon}{\rho_0}, \quad P = \frac{\bar{P} - \bar{P}_\epsilon}{\rho_0 U_0^2}, \quad S = \frac{\bar{S}}{S_0}, \quad S^\circ = \frac{\dot{S} D}{\rho_0 U_0 S_0}, \quad Q^\circ = \frac{\dot{Q} D}{\rho_0 U_0 T_0 C_{po}}$$

(1)

Here, the subscript o denotes reference quantities, and the subscript ϵ represents the hydrostatic equilibrium conditions. It is noted here also that S_0 is simply a convenient reference concentration. The resulting non-dimensionalized equations, under the assumptions of no chemical reaction,
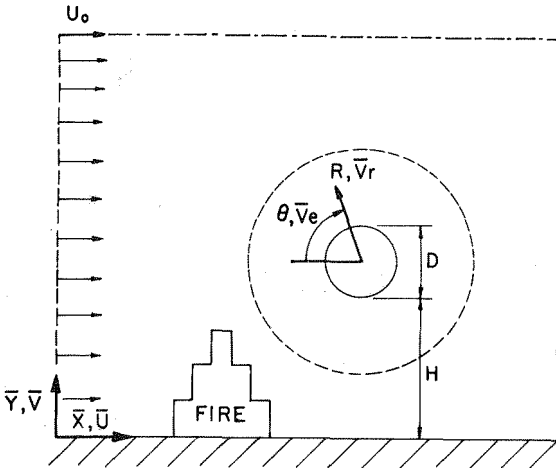

FIGURE 1. Coodinate System

negligible viscous dissipation and pressure work, and representations of turbulent flux quantities by means of effective (laminar plus turbulent) transport properties, can now be written as (Yang et al, 1984; Kou, 1984)

$$\frac{\partial \rho}{\partial t} + \frac{\partial (\rho U)}{\partial X} + \frac{\partial (\rho V)}{\partial Y} = 0 \tag{2}$$

$$\frac{\partial (\rho U)}{\partial t} + \frac{\partial (\rho U^2)}{\partial X} + \frac{\partial (\rho UV)}{\partial Y} = \frac{\partial}{\partial Y} \left[\frac{1}{Re_e} \left(\frac{\partial U}{\partial Y} + \frac{\partial V}{\partial X} \right) \right]$$

$$+ \frac{\partial}{\partial X} \left(\frac{4}{3 \, Re} \frac{\partial U}{\partial X_e} - \frac{2}{3 \, Re} \frac{\partial V}{\partial Y_e} \right) - \frac{\partial P}{\partial X} \tag{3}$$

$$\frac{\partial (\rho V)}{\partial t} + \frac{\partial (\rho UV)}{\partial X} + \frac{\partial (\rho V^2)}{\partial Y} = \frac{\partial}{\partial X} \left[\frac{1}{Re_e} \left(\frac{\partial U}{\partial Y} + \frac{\partial V}{\partial X} \right) \right]$$

$$+ \frac{\partial}{\partial Y} \left(\frac{4}{3 \, Re_e} \frac{\partial V}{\partial Y} - \frac{2}{3 \, Re_e} \frac{\partial U}{\partial X} \right) - \frac{\partial P}{\partial Y} - (\rho - \rho_\varepsilon) \frac{gD}{U_o^2} \tag{4}$$

$$\frac{\partial (\rho T)}{\partial t} + \frac{\partial (\rho UT)}{\partial X} + \frac{\partial (\rho VT)}{\partial Y} = \frac{\partial}{\partial X} \left(\frac{1}{Re_e \, Pr_e} \frac{\partial T}{\partial X} \right)$$

$$+ \frac{\partial}{\partial y} \left(\frac{1}{Re_e \, Pr_e} \frac{\partial T}{\partial Y} \right) + Q^\circ \tag{5}$$

$$\frac{\partial (\rho S)}{\partial t} + \frac{\partial (\rho US)}{\partial X} + \frac{\partial (\rho VS)}{\partial Y} = \frac{\partial}{\partial X} \left(\frac{1}{Re \, Sc_e} \frac{\partial S}{\partial X_e} \right)$$

$$+ \frac{\partial}{\partial Y} \left(\frac{1}{Re_e Pr_e} \frac{\partial S}{\partial Y} \right) + S^\circ \tag{6}$$

$$\rho T = \frac{U_o^2}{R_o T_o} P + P_\varepsilon \tag{7}$$

$$\rho_\varepsilon = \exp \left[- \left(\frac{gD}{R_o T_o} \right) Y \right] \tag{8}$$

where Re_e, Pr_e, and Sc_e are the local effective Reynolds number, Prandtl number, and Schmidt number, respectively, defined by

$$Re_e = \frac{\rho_o U_o D}{\bar{\mu}_{eff}} \quad , \quad Pr_e = \frac{\bar{\mu}_{eff} C_p}{\bar{k}_{eff}} \quad , \quad Sc_e = \frac{\bar{\nu}_{eff}}{\bar{D}_{eff}} \tag{9}$$

where $\bar{\mu}_{eff}$, $\bar{k}_{eff}$ and $\bar{D}_{eff}$ are the effective (laminar plus turbulent) viscosity, conductivity and mass diffusion coefficient, respectively. It is understood that both Q° and S° are taken to be zero outside the flame envelope.

Before the above equations can be solved, closure models for the turbulent transport properties must be introduced. In the present study, an algebraic

turbulence model for recirculating buoyant flows with wide variations in the turbulence level, which accounts for both local shear and stratification effects, is employed (Nee and Liu, 1978). It is given in a non-dimensional form by

$$\mu_{eff} = \frac{\bar{\mu}_{eff}}{\mu_o} = 1 + \frac{[(\frac{\partial U}{\partial Y})^2 + (\frac{\partial V}{\partial X})^2]^{1/2} (\frac{\ell}{D})^2}{2 + \frac{Ri}{Pr_t}} \tag{10}$$

where μ_o is the reference molecular viscosity and ℓ is a mixing length given by

$$\frac{\ell}{D} = K \{ \frac{(U^2 + V^2)^{1/2}}{[(\frac{\partial U}{\partial X})^2 + (\frac{\partial U}{\partial Y})^2 + (\frac{\partial V}{\partial X})^2 + (\frac{\partial V}{\partial Y})^2]^{1/2}}$$

$$+ \frac{[(\frac{\partial U}{\partial X})^2 + (\frac{\partial U}{\partial Y})^2 + (\frac{\partial V}{\partial X})^2 + (\frac{\partial V}{\partial Y})^2]^{1/2}}{[(\frac{\partial^2 U}{\partial X^2})^2 + (\frac{\partial^2 U}{\partial Y^2})^2 + (\frac{\partial^2 V}{\partial X^2})^2 + (\frac{\partial^2 V}{\partial Y^2})^2]^{1/2}} \} \tag{11}$$

where K is an adjustable constant and Ri is the gradient Richardson number given by

$$Ri = \frac{gD(\frac{\partial T}{\partial Y})}{U_o^2 (\frac{\partial U}{\partial Y})^2} \tag{12}$$

Furthermore, the effective conductivity $\bar{k}_{eff}$ and effective mass diffusion coefficient $\bar{D}_{eff}$ are related to the effective viscosity $\bar{\mu}_{eff}$ by

$$\frac{1}{Pr_e} = \frac{\bar{k}_{eff}}{\bar{\mu}_o C_p} = \frac{1}{Pr} + \frac{1}{Pr_t} (\mu_{eff} - 1) \tag{13}$$

$$\frac{1}{Sc_e} = \frac{\rho_o \bar{D}_{eff}}{\bar{\mu}_o} = \frac{1}{Sc} + \frac{1}{Sc_t} (\mu_{eff} - 1) \tag{14}$$

where Pr and Sc are the molecular Prandtl and Schmidt numbers, respectively. In the present study, both the turbulent Prandtl number Pr_t and the turbulent Schmidt number Sc_t are taken to be unity.

The governing equations (2) through (8) and the turbulence model given in Eqs. (10) through (12) can be similarly written for the cylindrical coordinate system by noting that

$$U = - V_r \cos\theta + V_\theta \sin\theta \tag{15}$$

$$V = V_r \sin\theta + V_\theta \cos\theta \tag{16}$$

and the corresponding coordinate relations as represented in Figure 1, and they have been given by Kou (1984). For the sake of conserving space, they will not be repeated here. The geometrical linking of the two coordinate systems will be described later. The boundary conditions are easily prescribed. The velocity components on the ground and around the cylinder surface are zero, and the velocity U along X=0 is uniform at U_o. Theoretically, the solution regions are infinitely extended in both positive X and Y directions. The heat and smoke source located inside the flame envelope provides the driving force for the

temperature and smoke concentration fields. The ground and the cylinder (fuselage) surface are taken to be thermally insulated, and at the same time there is no net smoke particle deposition there. Temperatures and smoke concentrations away from the heat source including those along X=0 are taken to be ambient at T_0 and S=0, respectively.

In the present study, the governing equations, subjected to the boundary conditions described above, have been solved numerically by finite differences based on a micro-control volume scheme with primitive variables originally introduced by Patankar and Spalding (1972) in a manner similar to that used in an earlier companion study dealing with aircraft cabin fires (Yang et al, 1984). However, the formulations of the finite-difference equations and the associated calculation algorithm are more complicated due to the hybrid (rectangular and cylindrical) grid system used. Details of the numerical scheme are given by Kou (1984) and also contained in a companion paper (Kou, Yang and Lloyd, 1985), together with the results of validation studies based on this numerical scheme. It suffices here to describe briefly several of the salient features of the numerical computations.

A typical calculation grid system for H/D = 1.0 is shown in Figure 2. It is seen that the circular cylinder is deliberately placed close to the left lower corner of the computational grid to accommodate the extent of the thermal plume in the region above the fire and shedding of the flow behind the cylinder. The boundary conditions at the top and right free boundaries are prescribed as follows: The gradients for both velocity components normal to the boundary are taken to be zero. Also at any point along either of the free boundaries, the gradients of temperature and smoke concentration are also taken to be zero if the flow is outward, and when the flow is inward, ambient values of T and S, i.e. T=1 and S=0 are specified at that point. These are sometimes known as the natural boundary conditions.

One unique feature of the grid system used here is the hybrid mesh depicted in Figure 2. While the computations in either the rectangular grid or the cylindrical grid can be carried out in a standard manner, overlapping interfacial cell regions are provided to allow continuation of calculations from one region into the other. Even though the present study is only concerned with long-time behaviors, calculations marching in time are carried out until the long-time solution is achieved. Within each time step, finite-difference solutions for the two coordinate regions are obtained alternately until
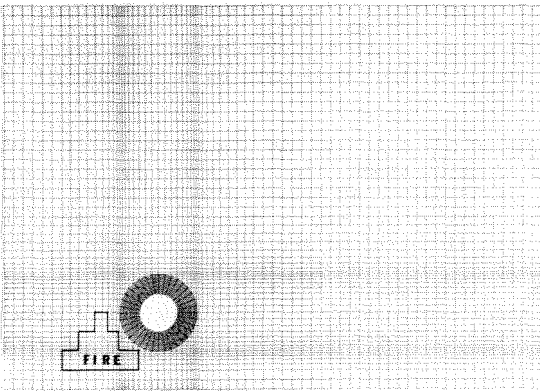

FIGURE 2. The Grid for the Case of Height Ratio H/D = 1.0.

convergence is reached. Calculations for each region are based on the conditions at the interface cells, and these values can be transferred from one region to the other by using standard bilinear interpolation formulae. Within each coordinate region, the computations proceed in a manner identical to that described by Yang et al (1984) and hence will not be repeated here. It is however important to note that the procedure does utilize upwind differencing for the convective terms and hence numerical errors due to false diffusion can be expected at large cell Peclet numbers (Patankar, 1980). However, due to relatively large effective viscosities encountered in the present problem, the cell Peclet number is found to be reasonably small, indicating that the effect of false diffusion should also be small.

The validity of the entire calculation procedure, including the part that deals with iterations involving both coordinate regions, has been established by a series of validation studies. Results of these studies have been given by Kou (1984), and are also included in a paper describing the details of the numerical procedure (Kou, Yang and Lloyd, 1985).

As will be described later, results for the buoyancy-dominated situations all show long-time oscillatory behaviors in the flow field. A question rises then as to whether such oscillatory behaviors are physically real. There are pervasive reasons that they are indeed real. The full-scale tests at the Technical Center of the U. S. Federal Aviation Administration also showed large-scale oscillations (Eklund, 1981). In preliminary calculations utilizing much coarser grid systems, such oscilltions have also been found (Kou, 1984). Even though no three-dimensional calculations have been made, there is evidence that the oscillatory flow field is predicted by both two-dimensional and three-dimensional calculations (Satoh et al, 1983). The resulting oscillatory frequencies are very similar, while the amplitudes for the three-dimensional cases are smaller. This is expected in view of the fact that two-dimensional flows are generally more stiff. Finally, it has also been found that the Richardson number in the turbulence model, equation (12), is important and affects both the frequency and amplitudes of the oscillations.

RESULTS OF SIMULATION STUDIES

The numerical procedure mentioned above is utilized in a series of simulation studies to determine the combined effects of the buoyant flow due to the fire and smoke source and the forced flow due to the prevailing wind speed on the velocity, temperature and smoke concentration fields in the neighborhood of the fuselage as a function of the wind speed and the elevation of the fuselage from the ground. Of particular interest is the resulting pressure variations, and smoke concentrations around the fuselage, since these are the physical parameters that will determine the fire and smoke hazards inside the aircraft cabin, if there is an opening present in the fuselage as a result of a survivable aircraft accident.

With reference to Figure 2, the diameter of the fuselage is taken to be 3.05 meters (10 feet), and the corresponding calculation domain is given by X=13 and Y=9. The center of the fuselage is located at X=3.5 from the left free boundary. The depth of the field is arbitrarily taken to be 6.10 meters (20 feet) and is only used to determine the strengths of the fire and smoke source in accordance with the full-scale tests performed at the Technical Center of the U.S. Federal Aviation Administration. As a result, the fire source is taken to be at a constant strength and has a total power output of 75,887 kw and a total rate of smoke generation of 0.1314 kg/sec, corresponding to that for a very

dirty fire. The location of the fire is taken to be fixed, and the fire
envelope shape is also fixed as shown in Figure 2 to approximate that for a real
fire. This approximation may indeed not be too realistic, especially in cases
where the forced flow is strong. However, since the effect of the cross flow on
the flame slope is not a priori known, it is difficult to model. This can only
be remedied by introducing a combustion model in the calculations. Simulation
studies have been carried out for fuselage elevations of H/D = 0.5, 1.0 and 1.5
and wind speeds of 3.05 m/sec (10 ft/sec), 6.10 m/sec (20 ft/sec) and 9.14 m/sec
(30 ft/sec). Calculations have alseo been carried out for the case of zero wind
speed corresponding to pure natural convection or fire plume situations and the
case of zero heat input which corresponds to pure forced flow over a circular
cylinder near a ground. Detailed results have been given by Kou (1984).   Since
the limited space here does not permit their full presentation, only selected
results are given in the following:

Before these results are presented, however, it is expedient here to make
several general observations to facilitate the physical interpretation later on.
Firstly with the prescribed heat source, the range of wind speeds covered in
this study does span the complete region of interest ranging from forced-flow
dominated situations (9.14 m/sec) to natural-convection dominated flow (3.05
m/sec).   Secondly, forced flow tends to stabilize the flow, while the buoyancy
effect due to the fire source destabilizes it. Thirdly, strong buoyancy effects
lead to long-time behaviors which are oscillatory, while time-independent
steady-state behaviors are obtained when forced-flow effects are dominant.
Fourthly, for elevation parameters H/D exceeding unity, the ground effect is not
significant. For H/D less than unity, the reduction in local flow area and the
ground friction become increasingly important and generally have the opposite
effects on the flow field.   Lastly, in view of the similarity of the governing
equations and the boundary conditions, results for the temperature field are
very similar to that for the smoke concentration field.   Consequently, separate
physical interpretations of these two fields are not necessary.

Figures 3(a) and (b) are typical smoke concentration contour plots for the case
of H/D = 0.5.   Figure 3(a) is for a wind speed of 3.05 m/sec (10 ft/sec) and
Figure 3(b), for the speed of 6.10 m/sec (20 ft/sec).   In both cases, buoyancy
effects are significant and long-time behaviors are oscillatory due essentially
to the instability of the fire plumes.   The absolute time instants noted in
these figures have no special meaning, other than that reflecting the period
duing the oscillations.   At the lower speed in Figure 3(a), the effect of the
wind on the fire plume is still minimal, and the fuselage is not much affected
by the fire.   The temperatures on the surface are essentially ambient. When the
wind speed is doubled (Figure 3(b)), the fire plume is swept in the direction of
the wind and the fuselage is largely engulfed by the fire.   This represents the
situation where both forced flow and natural convection play equally important
roles.   As already noted previously, similar oscillatory behaviors of the smoke
field have been observed in the full-scale tests at the Technical Center of the
U. S. Federal Aviation Administration (Eklund, 1981).   Unfortunately no direct
comparisons can be made because of the qualitative nature of the tests.

One important result in the present study, as pointed out previously, is the
pressure variation around the fuselage. Figure 4 describes such pressure
variations at θ = 0° and 180° for H/D = 0.5 and a wind speed of 9.14 m/sec (30
ft/sec).   It is seen that the buoyancy effect induces a regular oscillation in
the long-time behavior and the period is about 4 seconds.   Additionally, it has
been found that the pressure depressions at the bottom of the fuselage are
higher than that at the top.   It is believed that the buoyancy in the fire
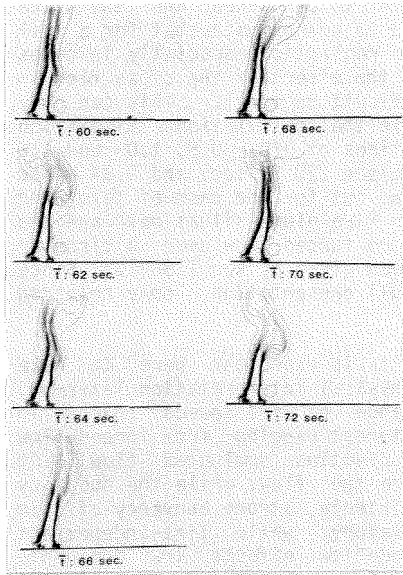
(a) U_0 = 3.05 m/sec
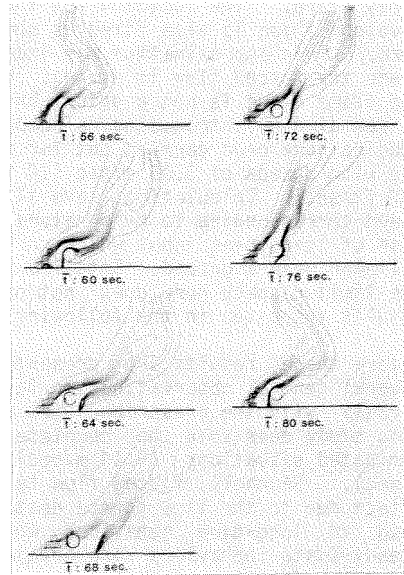
(b) U_0 = 6.10 m/sec

FIGURE 3. Oscillatory Smoke Concentration Fields for H/D = 0.5.

accelerates the flow more in the region below the fuselage, causing the pressure to decrease there, despite the slight drag offered by the presence of the ground. Figure 5 shows the effect of reducing the wind speed from 9.14 m/sec (30 ft/sec) to 6.10 m/sec (20 ft/sec) at the same fuselage elevation H/D = 0.5. The increased buoyancy effect in this case further destabilizes the flow and the long-time oscillatory behavior is no longer very regular. The presence of the ground seems to damp out some of the oscillations in the region below the
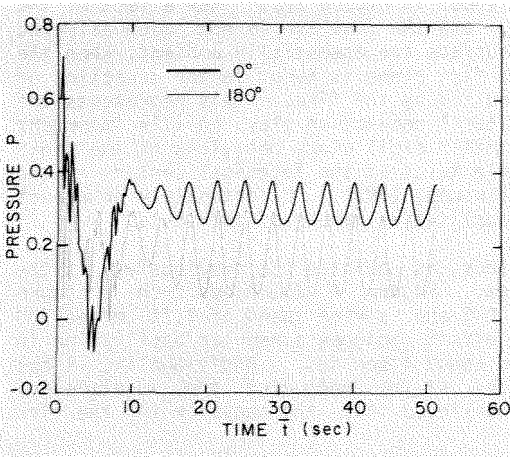

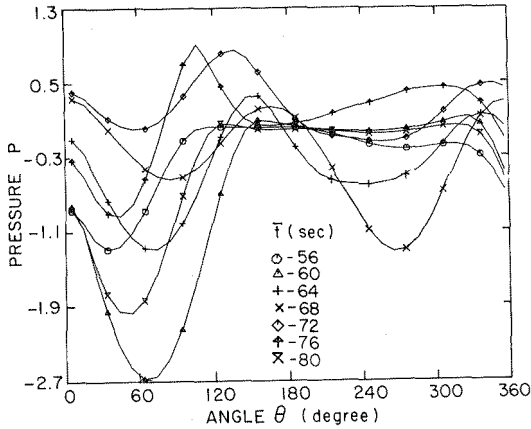FIGURE 4. Pressure at θ = 0° and 180° for U_0 = 9.14 m/sec and H/D = 0.5 (Heat On).

FIGURE 5. Pressure Variation Around Fuselage for U_0 = 6.10 m/sec and H/D = 0.5 (Heat Source On).

fuselage.   From Figure 5 and Figure 3(b) , which depict the corresponding field behaviors, the period of oscillation can be approximately estimated at 24 seconds, and a more exact value can only be determined by performing a Fourier analysis of the irregular oscillations.   Figure 6 shows the corresponding pressure variations for a case similar to that in Figure 8 except that the fuselage elevation is now increased to H/D = 1.5   Somewhat irregular oscillations are still present, but the behavior at the bottom and at the top of the fuselage are no longer that different, again attesting to the fact that for this value of H/D the ground loses much of its effect on the flow field.   For this case, an approximate period is estimated at 28 seconds.

Figure 7 gives an illustration concerning the temperature variations around the fuselage, and it is understood that this same information can be interpreted as the smoke concentration variations.   However, it should also be understood that T=1 would then correspond to S=0.   Figure 10 is for the case of H/D = 0.5 and a wind speed of 6.10 m/sec (20 ft/sec).   Here the wind speed sweeps the fire toward the fuselage, more under it than above.   As a result, the temperatures are higher at the lower surface of the fuselage.   It is also seen that during certain times in the cycle the fire plume actually stays away from the fuselage,
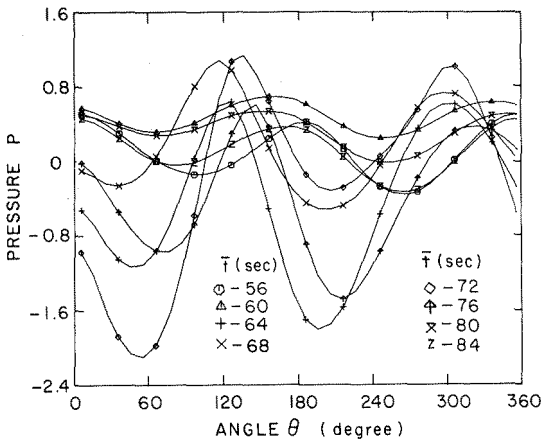

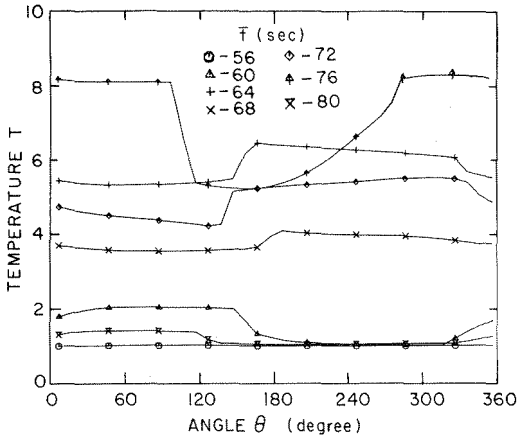FIGURE 6. Pressure Variations Around Fuselage for U_0 = 6.10 m/sec and H/D = 1.5 (Heat Source On).

181

FIGURE 7. Temperature Variation Around Fuselage for U_0 = 6.10 m/sec and H/D = 0.5 (Heat Source On).

thus leaving the entire fuselage surface at essentially the ambient temperature. Also, during the other parts of the cycle, the surface temperature can become very high, especially at the front of the fuselage.

CONCLUDING REMARKS

A numerical study based on two-dimensional finite-difference calculations with a hybrid grid system has been carried out to study the effects of wind speed and elevation of an aircraft fuselage located downwind of a fire and smoke source on the pressure, temperature and smoke concentration variations at the surface of the fuselage. The following general conclusions can be drawn:

(a) The surface variations in pressure, temperature and smoke at the fuselage are very sensitive to the relative effects of the prevailing wind speed and the buoyant flow from the fire source. The buoyancy arises from the fire source destabilizes the flow, and causes the long-time behavior to become oscillatory. When the buoyancy effect is large, the oscillations can become rather irregular.

(b) For elevation parameters exceeding H/D = 1.0, the ground does not exert much effect on the physical characteristics in the immediate neighborhood of the fuselage. As H/D falls below unity, the ground effect becomes increasingly more important, especially when the fire is present.

The present study can only be considered as a first step in addressing the external fire problem in survivable aircraft accidents. In the real scenario, the flow field is necessarily three-dimensional, and there is always thermal radiation exchange between the fire, the smoke, the ground and the fuselage. The combustion process involving the spilled fuel is also present in the real phenomena. Systematic studies, both numerical and experimental, are needed to address these realistic effects so that the all important fire safety issues involved in survivable aircraft accident can be rationally dealt with.

NOMENCLATURE

C_p	isobaric heat capacity
D	cylinder diameter
D	mass diffusion coefficienbt
g	gravitational acceleration

182

H	fuselage elevation
K	constant
k	thermal conductivity
ℓ	mixing length
P	pressure
Pr	Prandtl number
$\dot{Q}$	volumetric heat generation rate
$Q°$	non-dimensional volumetric heat source strength
R	radius variable
Re	Reynolds number
Ri	Gradient Richardson number
R_o	gas constant
S	smoke concentration
Sc	Schmidt number
$\dot{S}$	volumetric smoke generation rate
$S°$	non-dimensional volumetric smoke source strength
T	temperature
t	time variable
U,V	velocity components in X, Y directions, respectively
U_o	reference velocity
V_r, V_θ	velocity components in R, θ directions, respectively
X,Y	Cartesian coordinates

Greek Symbols

θ	angle in cylindrical coordinates
μ	viscosity
ρ	density

Subscripts

e	based on effective transport properties
eff	effective (molecular plus turbulent)
o	reference quantities
t	turbulent
ε	hydrostatic equilibrium condition

Superscript

| — | dimensional quantities |

ACKNOWLEDGEMENT

REFERENCES

Eklund, T. (1981). personal communication.

Emmons, H. W. (1982). The ingestion of flames and fire gases into a hole in an aircraft cabin for arbitrary tilt angles and wind speed. Home Fire Project TR No. 52, Division of Applied Sciences, Harvard University, Cambridge, MA.

Kou, H. S. (1984). Turbulent buoyant flow and pressure variations around a circular cylinder in a cross uniform flow near the ground. Ph.D. dissertation, University of Notre Dame, USA, 233 pp.

Kou, H. S., Yang, K. T., and Lloyd, J. R. (1985). A numerical study of mixed convection for flow over a circular cylinder near a ground in the presence of a volumetric heat source. Paper under review for publication.

Nee, V. W. and Liu, V. K. (1978). An algebraic turbulence model for buoyant recirculating flow. Technical Report TR-79002-78-2, Dept. of Aerospace and Mechanical Engineering, University of Notre Dame, 107 pp.

Patankar, S. V. (1980). Numerical Heat Transfer and Fluid Flow, McGraw Hill Book Co.

Patankar, S. V. and Spalding, D. B. (1972). A calculation procedure for heat, mass and momentum transfer in three-dimensional parabolic flow, Int. J. of Heat and Mass Transfer, vol. 15, 1787.

Satoh, K., Yang, K. T., Lloyd, J. R. and Kanury, A. M. (1983). A Numerical Finite-Difference Study of the Oscillatory Behavior of Vertically Vented Compartments, Numerical Properties and Methodologies in Heat Transfer, Proc. 2nd Nat. Sym., ed. T. M. Shih, Hemisphere Publishing Corp., 517.

Yang, K. T., Lloyd, J. R., Kanury, A. M. and Satoh, K. (1984). Modeling of turbulent buoyant flows in aircraft cabins, Comb. Sci. and Tech., vol. 39, 107.